Carbothermally Prepared Nanophase SiC/ Si_3N_4 Composite Powders and Densified Parts

Daniel F. Carroll, Alan W. Weimer, Stephen D. Dunmead, Glenn A. Eisman, James H. Hwang, Gene A. Cochran, David W. Susnitzky, Donald R. Beaman, and Cynthia L. Conner
Ceramics & Advanced Materials Research, The Dow Chemical Company, Midland, MI 48667

Nanophase SiC/Si_3N_4 composite powders were synthesized by the carbothermal nitridation of SiO_2. These powders have desirable characteristics of high quality with oxygen contents on the order of 1.5 to 2 wt. %, surface area of ~ 10 m^2/g, submicron α-Si_3N_4, low metallic impurity levels, and a homogeneous distribution of the nanophase SiC phase. High-resolution TEM analysis has shown that the content and size of the nanophase SiC can be varied from 0.5 to 50 wt. % and 25 to 500 nm, respectively, through proper control of raw materials and reactor conditions. To determine how the nanophase SiC reinforcement affects the mechanical properties of Si_3N_4, densified components were fabricated using both pressureless and pressure-assisted densification methods. TEM analysis revealed that the nanophase SiC particles are distributed both intergranularly and intragranularly throughout the Si_3N_4 matrix. By controlling the sintering additive package and the sintering conditions, the ratio of inter- to intragranular SiC can be adjusted. Mechanical property measurements at elevated temperatures showed a dramatic improvement in high-temperature strength and creep resistance over components made with commercially available powders.

Introduction

Thermochemistry

Silicon nitride (Si_3N_4) and silicon carbide (SiC) can both be synthesized in the presence of nitrogen (N_2) by the carbothermal reduction of silica (SiO_2) according to the overall reactions:

$$3SiO_2 + 6C + 2N_2 \rightarrow Si_3N_4 + 6CO \quad (1)$$

$$SiO_2 + 3C \rightarrow SiC + 2CO. \quad (2)$$

Both reactions are moderately endothermic, requiring approximately 1,268 kJ/mol Si_3N_4 and 572 kJ/mol SiC at 1,427°C (1,700 K) and 1,827°C (2,100 K), respectively.

Both reactions are believed to involve multiple steps and to begin with the reduction of SiO_2 by carbon (C) in direct physical contact according to:

$$C + SiO_2 \rightarrow SiO + CO. \quad (3)$$

The reduction product of this first step is gaseous silicon monoxide (SiO), a volatile intermediate that then reacts to yield Si_3N_4 or SiC. Once CO is formed, SiO can also be produced by gas-phase carbon reduction according to the combination of Reactions 4 and 5 below:

$$SiO_2 + CO \rightarrow SiO + CO_2 \quad (4)$$

$$C + CO_2 \rightarrow 2CO \quad (5)$$

With SiO present, Si_3N_4 can form according to

$$3C + 3SiO + 2N_2 \rightarrow Si_3N_4 + 3CO \quad (6)$$

$$3SiO + 3CO + 2N_2 \rightarrow Si_3N_4 + 3CO_2 \quad (7)$$

(followed by Reaction 5).

On the basis of product morphology (single-crystal hexagonal prisms), Zhang and Cannon (1984) proposed that heterogeneous nucleation of Si_3N_4 proceeds according to Reaction 6, but that growth occurs by a gas-phase process according to

Correspondence concerning this article should be addressed to A. W. Weimer.
Present address for A. W. Weimer: Department of Chemical Engineering, University of Colorado, Boulder, CO 80309.

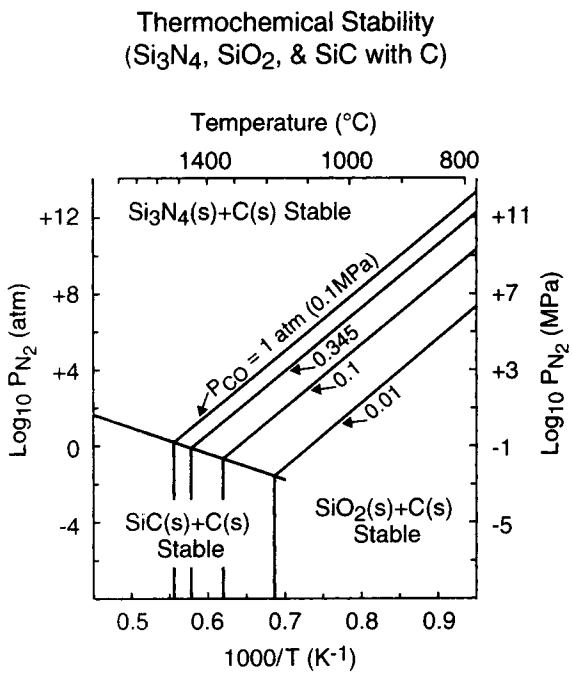

Figure 1. Thermochemical correlation for stability of Si_3N_4, SiO_2, and SiC coexisting with carbon.
Adapted from Yamaguchi, 1986.

Reaction 7. Although the exact reaction mechanism is undefined, there is general agreement that Si_3N_4 forms by a gas-phase reaction involving SiO.

Likewise, SiC is formed from SiO according to

$$2C + SiO \rightarrow SiC + CO. \quad (8)$$

Silicon nitride (Si_3N_4) synthesis is favorable (Yamaguchi, 1986) below a thermodynamically imposed upper reaction temperature limit (Figure 1). This temperature is estimated to be approximately $T = 1{,}435$°C at near atmospheric N_2 pressure, depending on the data used. Silicon carbide (SiC) is the stable species under coexistence with carbon above this temperature for $p_{N_2} = 0.1$ MPa (1 atm). Within a relatively narrow temperature window around this transition temperature, SiC grain growth is minimized and nanophase SiC crystallites are produced. It is in this temperature range that nanophase SiC/Si_3N_4 composite powders can be synthesized.

Nanophase SiC/Si_3N_4 composite properties

Over the last several years, the development of nanophase reinforced ceramic composites has received considerable attention due to the ability to form materials with enhanced physical and mechanical properties. One such composite material is nanophase SiC-reinforced Si_3N_4. Work by Niihara et al. (1993) has shown that the incorporation of nanometer-sized SiC particles into a Si_3N_4 matrix can lead to impressive increases in room temperature fracture toughness and strength (7 MPa·$m^{1/2}$ and 1.5 GPa, respectively) over the monolithic Si_3N_4 material. Nanophase SiC reinforcements in Si_3N_4 have also produced exceptional high-temperature strengths (1.0 GPa at 1,400°C) with minimal degradation up to temperatures of 1,500°C (Niihara et al., 1993), enhanced creep resistance (Hirano et al., 1996) and superior oxidation resistance up to 1,600°C (Riedel et al., 1995).

In these materials, the nanophase SiC particles are found to distribute themselves intergranularly in the glassy phase between the Si_3N_4 grains and intragranularly within the Si_3N_4 grains. Niihara et al. (1993) have suggested that the improvement in room temperature properties is due to the growth of fine, elongated Si_3N_4 grains caused by the nanophase SiC. This type of microstructure toughens the material and thereby increases the fracture strength via a crack-deflection toughening mechanism. The improved high-temperature mechanical properties have also been attributed to the intergranular SiC particles, minimizing the amount of grain boundary sliding and slow crack growth, and promoting the crystallization of the intergranular glass phase. The improved oxidation resistance is the result of a protective SiO_2 layer that forms on the surface of the composite. Even though other mechanisms for the improved properties have been proposed (Ishizaki and Yanai, 1995; Pezzotti and Sakai, 1994), there is a general agreement that nanophase composites do offer a performance advantage over their monolithic counterparts.

A significant effort has been placed on fabrication methods to make nanophase SiC/Si_3N_4 composite powders. Such approaches have included chemical vapor decomposition methods to make amorphous Si–C–N precursors (Niihara et al., 1989), pyrolysis of liquid organic precursors (Hapke and Ziegler, 1995), thermal decomposition of methane on submicron Si_3N_4 powders (Watari et al., 1988), the physical mixture of submicron SiC and Si_3N_4 powders (Drennan et al., 1995), and the carbothermal reduction of SiO_2 in the presence of nitrogen (Li et al., 1994; Matsui and Yamakawa, 1992; Carroll et al., 1995). All of these methods have been shown to produce composite powders that can be processed into components with improved properties.

Each of these methods has their advantages and disadvantages in the production of nanophase reinforced composites. For example, the CVD method described by Niihara et al. (1989) produces a composite material with a very uniform distribution of nanophase SiC. However, this approach requires the use of expensive raw materials. The approach of taking a physical mixture of submicron SiC and Si_3N_4 powder is more desirable in terms of raw material cost, but careful processing is necessary to obtain a homogeneous distribution of the SiC phase. It is believed that the carbothermal reduction of SiO_2 combines the advantages of both these methods, since low-cost raw materials are used and the cosynthesized product contains an inherently uniform distribution of nanophase SiC.

The preferred method for fabricating densified components from nanophase SiC/Si_3N_4 composite powders is through the application of gas-pressure sintering or hot-pressing densification methods. Akumine et al. (1992) have shown that pressure-assisted densification methods improve the sintered density and mechanical properties of nanophase composites compared to materials made by pressureless sintering methods. The presence of nanophase SiC is known to inhibit densification (Ramoul-Badache and Lancin, 1992) and the α to β transformation process (Sasaki et al., 1992). During pressureless sintering, this interaction between the nanophase SiC and the Si_3N_4/sintering additive system re-

sults in components with less than optimum mechanical properties. Therefore, pressure-assisted densification methods have primarily been used to facilitate densification and enable higher sintering temperatures to be reached to enhance the α to β transformation process and growth of β-Si_3N_4 grains.

There is a need to develop improved pressureless sintering methods for densifying nanophase SiC/Si_3N_4 composite powders into fully dense, high-quality fabricated components. The development of such methods requires a much better understanding of the interaction between the nanophase SiC and the glass phase during densification. Likewise, there is a need to understand the effect nanophase SiC content has on the densification process and the resulting part properties.

Objectives

This article presents the results of studies to synthesize nanophase SiC/Si_3N_4 composite powders by carbothermal reduction, the processing of these powders into densified nanophase SiC/Si_3N_4 parts, and the properties of the densified components. Of particular importance is the ability to control the amount and the crystallite size of nanophase SiC during the carbothermal reduction process. The effect of nanophase SiC on the pressureless sintering behavior of the composite powders is discussed with particular emphasis on the role sintering additive composition and crucible environment have on the stability of the SiC phase. Through this understanding of how the SiC phase interacts with the sintered body during densification, insight will be given on how to pressureless sinter nanophase SiC/Si_3N_4 composite powders into dense, high-strength components. The mechanical properties of nanophase SiC/Si_3N_4 components, densified by both pressureless sintering and hot-pressing methods, will be evaluated to determine the effect of nanophase SiC content on the room and elevated temperature properties.

Experimental Procedure

Composition of reactants

Aggregates having an average equivalent spherical diameter of approximately 8 mm (~ 5/16 in.) were prepared in various compositions made up of 100% excess carbon above the theoretical requirement according to overall Reaction 1. In some cases, "seed" α-Si_3N_4 was included in the precursor. The composition of additive "seed" varied in the ratio "seed"/SiO_2 = 0 to 0.6.

Preparation of nanophase Si_3N_4 from carbon and SiO_2 using excess carbon and containing additive "seed" Si_3N_4 can be described by

$$3SiO_2 + (6+x)C + 2N_2 + y\,Si_3N_4 \rightarrow (1+y)Si_3N_4 + 6CO + xC. \quad (9)$$

For 100% excess carbon, $x = 6$. For a ratio "seed"/SiO_2 = 0.6, $y = 0.77$. The method for preparing precursor aggregates is described elsewhere (Weimer et al., 1997). The raw materials carbon, silica, and "seed" Si_3N_4 are summarized in Table 1.

Apparatus, reaction procedure, and analytical powder characterization

The Si_3N_4 synthesis was carried out using an inductively heated rotating (3 rpm) crucible reactor (Figure 2). The reactor was large enough to react a 500-g batch of precursor aggregates, preparing sufficient product powder for post-processing and part fabrication. The reaction chamber was a 23-cm-ID × 23-cm-deep graphite crucible inclined at an angle of 22.5° with respect to horizontal. This crucible was placed in the center of an RF induction coil and attached to a molybdenum (Mo) shaft by which the crucible could be rotated. A total of six graphite lifts were attached to the inside of the crucible to aid in the mixing and turnover of the aggre-

Table 1. Chemical and Physical Analysis of Carbon, Silica, and "Seed" Si_3N_4

	Carbon			Silica	"Seed"
	C1‡	C2‡‡	C3§	SiO_2§§	Si_3N_4‖
wt. % C	98.6	98.9	96.0	n/m**	0.10
wt. % O	0.3	0.3	0.6	n/m	1.23
Crystallite d^*_{mecd} by TEM (nm)	30	220	60	n/m	110
d_{10} (μm)	n/m	n/m	n/m	2.36	0.35
d_{50} (μm)	n/m	n/m	n/m	10.2	0.66
d_{90} (μm)	n/m	n/m	n/m	24.9	1.35
S.A. (m^2/g)	72	8	25	0.4	10.1
% α phase	n/a†	n/a	n/a	n/a	> 90
ppm Al	n/d†† (< 50)	n/d (< 50)	32	n/d (< 50)	n/d (< 19)
ppm Ca	n/d (< 10)	n/d (< 10)	155	n/d (< 10)	n/d (< 2)
ppm Fe	n/d (< 15)	n/d (< 15)	40	n/d (< 15)	9

*Number average—mean equivalent circle diameter (d_{mecd}) (Russ, 1990).
**n/m = not measured.
†n/a = not applicable.
††n/d () = not detected at limit in parentheses.
‡C1: Shawinigan Black, Chevron Chemical Company.
‡‡C2: Thermax Ultra Pure, Cancarb Company.
§C3: Monarch 120, Cabot Corporation.
§§SiO_2 Source: Crystalline Quartz, Feldspar Company.
‖Seed Si_3N_4 Source: SNE10, Ube Chemical Company.

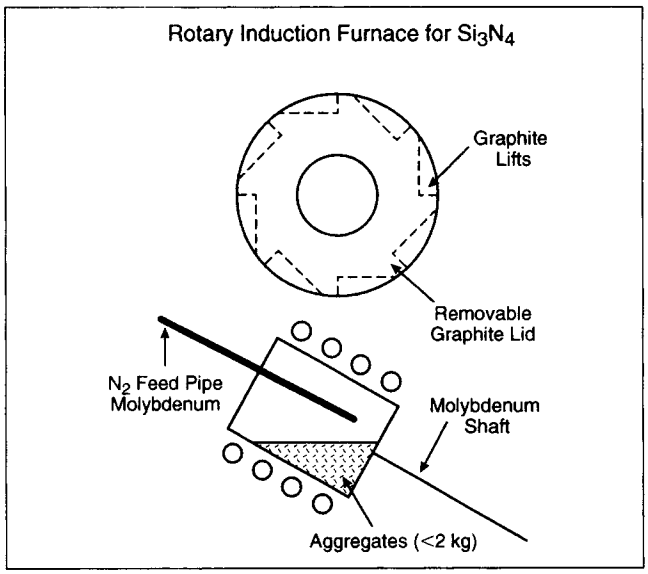

Figure 2. Rotary graphite crucible reactor.

gates during their heat treatment. After purging the reactor with N_2 gas (40 L/min) for 1 h, the crucible was heated at 30°C/min up to the desired reaction temperature as measured by a W-Re thermocouple located in the center of the crucible. The N_2 gas continued to flow at the 40-L/min rate throughout the reaction. Reaction temperature was maintained for the desired length of time and then the reactor was allowed to cool naturally.

Following reaction, the excess free carbon was removed by oxidation to CO_2. The reacted aggregates were placed in a quartz boat and heat treated in a tube furnace. A mixture of air and N_2 (50/50) flowed through the tube at a rate of 20 L/min. Oxidation was carried out for 3 h at 800°C. After the oxidation step, all remaining carbon in the product was assumed to be SiC, the presence of which was verified by X-ray diffraction.

Carbon analysis of the synthesized Si_3N_4 was carried out using a LECO HF 400 and LECO IR 412 Carbon Determinator (LECO Corporation). Sample material was combusted with released CO converted to CO_2 in a rare earth copper oxide catalytic heater. Carbon was then measured as CO_2 by IR analysis. Reaction product analysis for oxygen was completed using a LECO EF 400 and a LECO 436 Oxygen/Nitrogen Determinator. The sample was pyrolyzed and released oxygen combined with carbon to form CO. The CO was converted to CO_2 as described earlier and the oxygen was measured by IR in the form of CO_2.

The Si_3N_4 powder morphology was examined by field-emission gun scanning electron microscopy (FEG/SEM) using a Topcon DS-130F operated at 2.0–3.0 kV and by analytical transmission electron microscopy (ATEM) using a Topcon EM-002B operated at 200 kV. A mean number crystallite diameter [mean equivalent circle diameter (d_{mecd}), after Russ (1990)] was determined using randomly obtained TEM micrographs. The powder particles to be sized were selected by overlaying a grid onto each micrograph and then measuring the size of particles that were intersected by the grid.

Surface area was determined by the BET nitrogen adsorption method using an Autosorb-1 (Quantochrome Corp.) Surface Area Analyzer and following standard manufacturer's procedures. Trace metal impurities were quantified by X-ray fluorescence using a Kevex 0700 XRF spectrometer with analysis carried out using a Philip's PW1404 XRF spectrometer for metals. The XRF-11 Criss Software package was used for matrix corrections and to calculate the results. Particle-size distribution measurements (d_{10}, d_{50}, d_{90}) were made using a Microtrac II model 158705 Particle Size Analyzer (Leeds & Northrup). Powder was first dispersed in DI water and sonicated using a Sonabox II (Artek Systems Corporation) sonicator. Crystal-phase purity was determined by X-ray diffraction (Ragaku "Miniflex" X-ray Diffractometer).

Evaluation of composite powders in densified nanophase SiC/Si_3N_4 components

In order to characterize the effect of the nanophase SiC on the properties of densified components, the carbothermally produced nanophase SiC/Si_3N_4 powders were processed and densified. Sintering additives were wet milled in water or ethanol using an attritor mill and Si_3N_4 grinding media. Typical attrition times were on the order of 1 h at a rotation speed of 300–400 rpm. After milling, the slurry was either dried into a formulated powder using a rotoevaporator or directly cast into greenware using a slip-casting method and plaster molds. If the slurry was dried, greenware was fabricated by uniaxially pressing the powder in a 2.2-cm (7/8-in.)-diameter die at ~100 MPa (15,000 psig). Four different sintering additive formulations were used in this study.

The first two formulations examined the densification behavior of composite powders under pressureless sintering conditions. These formulations were selected from the Y_2O_3–MgO–SiO_2–ZrO_2 and the Y_2O_3–Al_2O_3–SiO_2 systems, respectively. Pressureless sintering was carried out in a graphite furnace under flowing N_2 conditions. Two types of crucible environments were utilized: (1) a solid BN crucible with lid, and (2) a graphite crucible with lid, where the greenware was embedded directly into a powder bed of the same Si_3N_4 composition. For the BN crucible configuration, greenware loading in the crucible was maximized so that the amount of weight loss experienced by each component during sintering would be minimal. During the pressureless sintering experiments in the BN crucible environment, a carbon monoxide (CO) analyzer (Beckman Industrial Corp.) measured the CO concentration in the N_2 atmosphere during densification. For the Y_2O_3–MgO–SiO_2–ZrO_2 system, the specimens were sintered at 1,750°C for 1 to 12 h at a heating rate of 5°C/min. The Y_2O_3–Al_2O_3–SiO_2 system was sintered at temperatures ranging from 1,650° to 1,815°C for times ranging from 1 h to 12 h.

The third and fourth formulations investigated were a Y_2O_3-based and a Y_2O_3–MgO–CaO-based composition. These formulations determined the effect of SiC content on the mechanical properties of the nanophase SiC/Si_3N_4 composites. These compositions were densified into billets ~5.1 ×7.6 cm (2 in. × 3 in.) in size by a hot-pressing method at temperatures of 1,800–1,850°C under an applied pressure of ~35 MPa (5,000 psig) for 60 to 90 min.

As a comparison to the composite powder produced from carbothermal reduction reaction, nanophase SiC/Si_3N_4 composite powders were also fabricated from a physical mixture

of a submicron-sized SiC powder (BSC21, Ferro Corporation) and a submicron-sized di-imide Si_3N_4 powder (SNE10, Ube Industries). This work was conducted to systematically determine how the presence of SiC affected densification and the resulting mechanical properties of nanophase-reinforced composite parts. In the evaluation of the densification behavior, a high-temperature dilatometer (Theta Industries) was used to characterize the shrinkage of these composites during sintering. The dilatometry study consisted of heating green compacts up to 1,750°C at 5°C/min under flowing N_2 and then holding at temperature for 1 h.

After densification, the nanophase SiC/Si_3N_4 composite parts were sectioned into specimens for microstructural and mechanical property analyses. The microstructures of each material were analyzed with SEM and TEM. X-Ray diffraction was also utilized to determine the degree of α- to β-transformation during sintering and the presence of glass crystallization. The amount of α- and β-Si_3N_4 was calculated from the X-ray pattern according to the procedure described by Bowen et al. (1978). The carbon content of the sintered parts was also analyzed using the LECO IR412 Determinator. For this analysis, the sintered parts were crushed to a -60-mesh particle size. Fracture strength specimens were machined from the densified billets following the procedures described in ASTM Standard C1161-90. Both the room and elevated temperature strengths were measured on an Instron testing frame (Model 8562, Instron Corporation) equipped with a high-temperature furnace. The fracture toughness of each material was analyzed using the chevron-notched bend-beam method (Newman, 1984). The relative creep resistance was determined from the amount of strain that each high-temperature strength specimen exhibited at failure.

Results and Discussion

Effect of temperature on SiC content and crystallite size

A large batch of precursor aggregates was prepared made up of 100% excess of C1 carbon ($x = 6$) and a ratio of "seed"/$SiO_2 = 0.6$ ($y = 0.77$). The aggregates were divided into 500-g batches for reaction in the rotating crucible reactor. Each batch of aggregates was reacted for 390 min, oxidized to remove free carbon, analyzed for carbon and oxygen content, phase purity, and SiC d_{mecd} by image analysis. The results are summarized in Figures 3 (SiC content) and 4 (SiC d_{mecd}). Reaction temperature has a significant effect on both the content and size of the produced SiC. For a 1,450°C reaction temperature, the final product had a SiC content of 1.3 wt. % SiC (0.4 wt. % fixed C). This increased to 4.7 wt. % SiC at 1,475°C and 48.1 wt. % SiC at 1,500°C. The mean equivalent circle diameter (d_{mecd}) increased from $d_{mecd} = 35$ nm for a 1,450°C reaction temperature to 140 nm for a 1,475°C reaction temperature and 310 nm for a 1,500°C reaction temperature. The increased quantity of SiC for higher reaction temperatures is consistent with the thermochemical stability results shown in Figure 1.

Effect of carbon source on SiC content and crystallite size

Three separate batches of precursor aggregates were prepared from a 100% excess of C1, C2, and C3 carbon ($x = 6$) and no "seed" Si_3N_4 ($y = 0$). Each batch of aggregates was reacted at 1,435°C for 5 h, oxidized to remove free carbon,

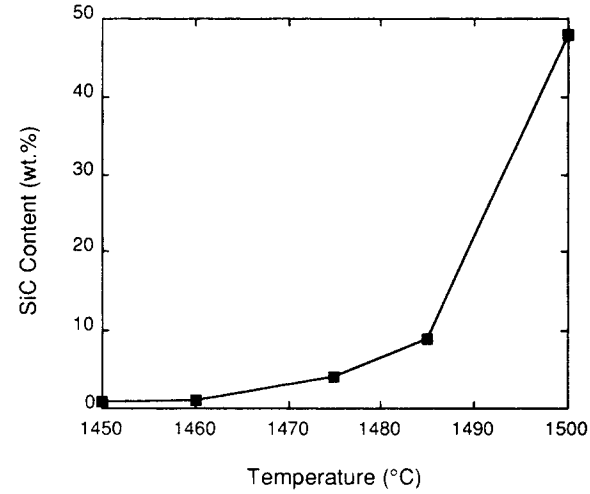

Figure 3. Effect of temperature on wt. % SiC content.
$t = 390$ min; 100% excess carbon; "seed"/$SiO_2 = 0.6$.

analyzed for carbon and oxygen content, phase purity, and SiC d_{mecd} by image analysis. All samples were analyzed by X-ray powder diffraction which showed the Si_3N_4 to be > 95% α-Si_3N_4. The product powder properties are summarized in Table 2.

Clearly, the size of the resulting SiC is highly dependent on the size of the starting carbon for high-purity carbon sources. Larger carbon crystallites yield larger SiC crystallites while smaller carbon crystallites yield smaller SiC crystallites. This effect has been reported previously for processes targeting pure SiC manufacture (Kennedy and North, 1983; Kevorkijan et al., 1989, 1992; Klinger et al., 1972; Wei et al., 1984; Weimer et al., 1993). The larger SiC crystallites produced from the C3 carbon source may be the result of grain growth promoted by metallic impurities in the carbon (see Table 1). The nanophase $d_{mecd} = 80$ nm SiC crystallites (synthesized from C3-containing precursor) are seen surrounding larger blocky α-Si_3N_4 crystallites in Figure 5. The α-Si_3N_4 particle characterization has been presented elsewhere (Weimer et al., 1997).

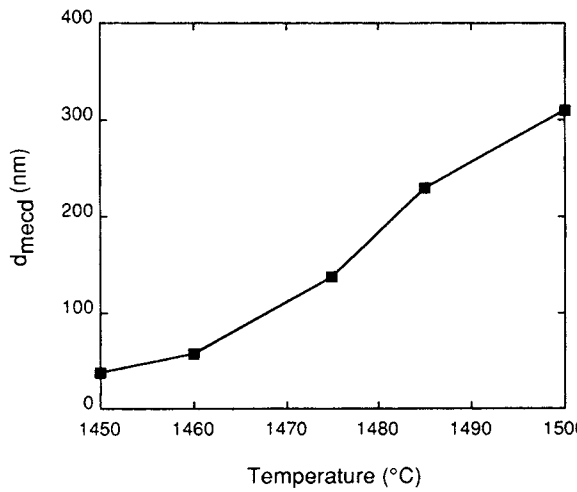

Figure 4. Effect of temperature on SiC mean equivalent circle diameter d_{mecd} (nm).
$t = 390$ min; 100% excess carbon; "seed"/$SiO_2 = 0.6$.

Table 2. Effect of Carbon Source on Nanophase SiC Content and Size ($x = 6$, $y = 0$; 5 h @ 1,435°C)

Carbon Source	wt. % O	wt. % C	wt. % SiC	wt. % Si_3N_4	SiC, d_{mecd} (nm)	SiC, d_{ecd} Range (nm)
C1	3.1	1.1	3.7	90.5	50	30–100
C2	4.2	1.8	6.0	86.1	90	70–150
C3	2.1	4.4	14.7	81.4	80	30–100

Pressureless sintering behavior of nanophase SiC/Si_3N_4 composite powders

The pressureless sintering behavior of two carbothermal SiC/Si_3N_4 powders with a SiC content of 1.9 and 3.8 wt. %, respectively, was initially examined with the Y_2O_3–MgO–SiO_2–ZrO_2 sintering formulation to determine how the residual SiC content affected densification. These powders contained greater than 95 wt. % α-Si_3N_4 and had a surface area of 9–10 m^2/g and a residual oxygen content of ~1.9–2.1 wt. %.

The greenware was sintered at 1,750°C for 1, 3, and 9 h using the BN crucible environment. The sintered densities and the amount of α- to β-Si_3N_4 transformation were characterized for each sample and are summarized in Figures 6 and 7, respectively. Both powders could be pressureless sintered to greater than 99% of theoretical density after 9 h of sintering. For shorter sintering times, the composite powder that contained less nanophase SiC exhibited more densification than that containing the higher SiC content.

The difference in the densification rates is believed to be related to an interaction between the nanophase SiC and the glassy phase at elevated temperatures. A similar decrease in sintering behavior with increasing amounts of nanophase SiC has also been reported by Ramoul-Badache and Lancin (1992) and Sasaki et al. (1992). The effects of nanophase SiC on densification will be discussed later.

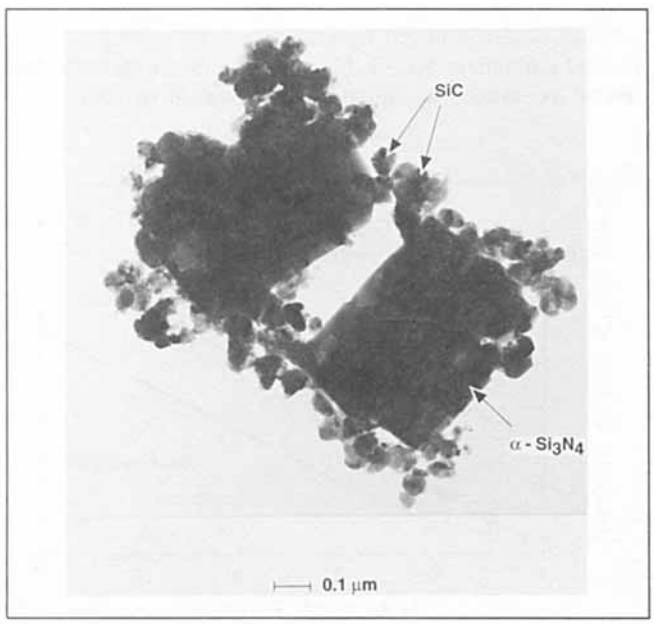

Figure 5. Nanophase SiC/Si_3N_4 composite powder produced from C3 carbon source by carbothermal nitridation.

5 h @ 1,435°C; 100% excess carbon; no "seed."

The degree of α- to β-transformation as a function of sintering time was also found to be dependent on the nanophase SiC content. The rate of α to β transformation was slower in the composite powder with the higher content of SiC. This reduction in the degree of α to β transformation has also been observed by Sasaki et al. (1992) during the densification of nanophase SiC/Si_3N_4 composites. Even though the reason for the decreased α to β transformation was unclear, their work did observe changes in the glass-phase chemistry. These changes in glass chemistry resulted in the crystallization of yttrium silicate compounds from the glass. Since the glass system is known to control the kinetics of the α to β transformation process (Hampshire and Jack, 1981), changes in glass content or composition by the SiC particles could result in a reduced α to β transformation process.

In order to investigate the possible reason for the reduced amount of densification with higher SiC contents, a controlled set of experiments was conducted on nanophase composite powders prepared by a physical mixture of submicron SiC and Si_3N_4 powders. In this study, 0 to 5 wt. % of SiC was added to a Si_3N_4 powder, which was then formulated with the same Y_2O_3–MgO–SiO_2–ZrO_2 composition. High-temperature dilatometry was initially utilized to examine how the shrinkage behavior of these composite powders varied with SiC content. The results are shown in Figure 8 for samples heated at 5°C/min to ~1,750°C. As the SiC content increased from 0 to 5 wt. %, the total amount of linear shrinkage decreased from ~16% to 11%. The differential shrinkage rates for each of these specimens are shown in Figure 9. These results indicate that the first sign of densification occurred at ~1,450°C and was independent of the SiC content.

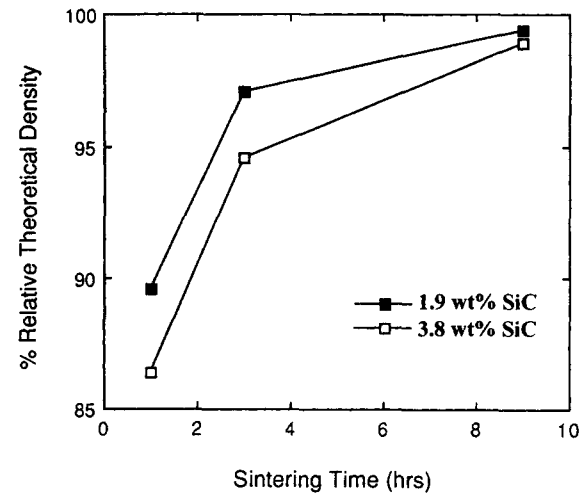

Figure 6. Sintered density as a function of sintering time at 1,750°C for carbothermal composite powders containing 1.9 and 3.8 wt. % SiC.

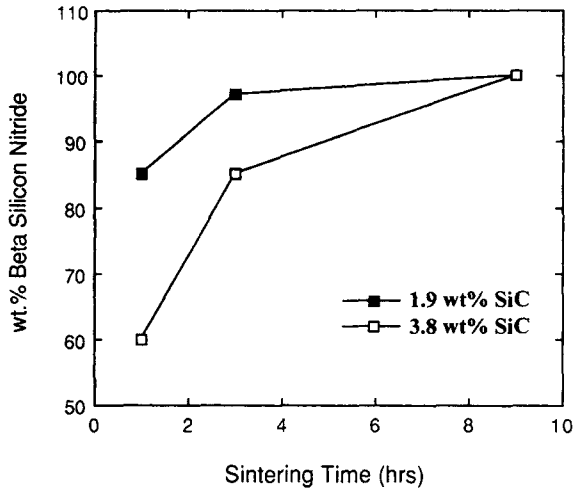

Figure 7. Beta Si_3N_4 content in pressureless sintered composite parts as a function of sintering time at 1,750°C for carbothermal composite powders containing 1.9 and 3.8 wt. % SiC.

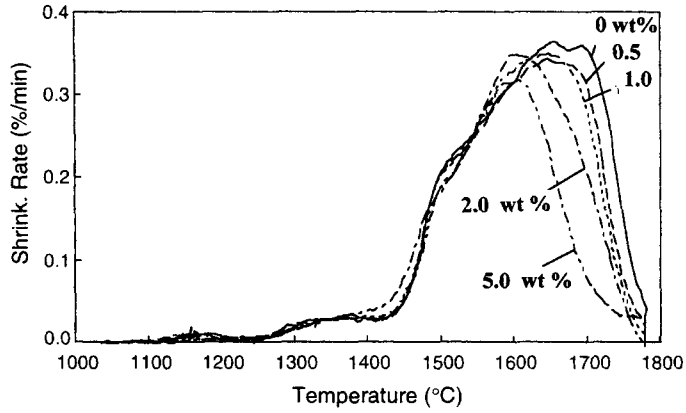

Figure 9. Dilatometry results showing the shrinkage rate as a function of temperature for physically mixed composite SiC/Si_3N_4 powders.

For temperatures above 1,600°C, the shrinkage rates dramatically decreased with increased amounts of SiC.

The same formulations were then sintered at 1,750°C for 12 h using both the BN and the graphite-crucible/powder-bed environments. For a low SiC content of 1.0 wt. %, both crucible environments yielded sintered densities > 99% of theoretical density. As the SiC content increased to 5.0 wt. %, the sintered densities decreased to 95.5% and 98.9% of theoretical density for the BN and the graphite crucible configurations, respectively. The 3.4% difference in sintered density at 5.0 wt. % SiC suggests that the crucible environment plays a key role in determining the behavior of the nanophase SiC during sintering.

The carbon content of the sintered components was then measured to determine how much of the SiC remained after densification. If SiC reacted during sintering to evolve CO gas, the residual carbon level in the densified component would be lower than the initial level in the starting formulation. The amount of residual carbon in each sintered component as a function of the initial SiC content is summarized in Figure 10. The dashed line indicates where the sintered residual carbon content should have fallen if no reaction occurred during densification. For the specimens sintered in the BN crucible, the residual carbon content was significantly lower than the initial levels. The specimens sintered in the graphite crucible with a powder bed exhibited a minimal decrease in the carbon content.

These results indicate that a significant reaction between the SiC and the Si_3N_4/sintering additive formulation occurred when sintering in the BN crucible environment, and essentially no reaction occurred when sintering in the graphite-crucible/powder environment. This reaction is responsible for the lower sintered density observed for the 5.0 wt. % SiC formulation densified in the BN crucible.

The effect of crucible environment on the stability of SiC was also observed in the formulations made with the carbothermal nanophase SiC/Si_3N_4 powders. For a carbothermal powder containing an initial carbon content of 0.48 wt. %

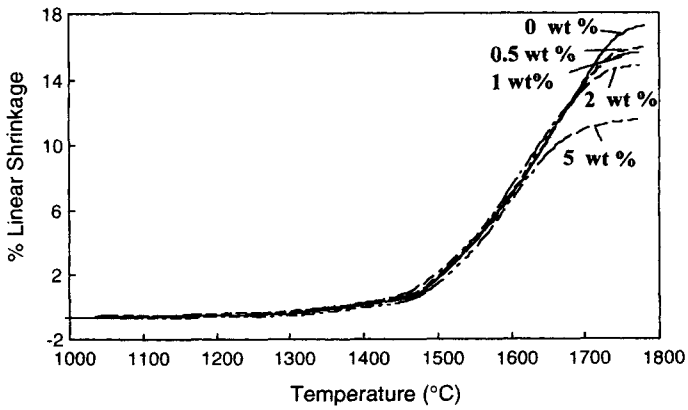

Figure 8. Dilatometry results showing the % linear shrinkage as a function of temperature for physically mixed composite SiC/Si_3N_4 powders.

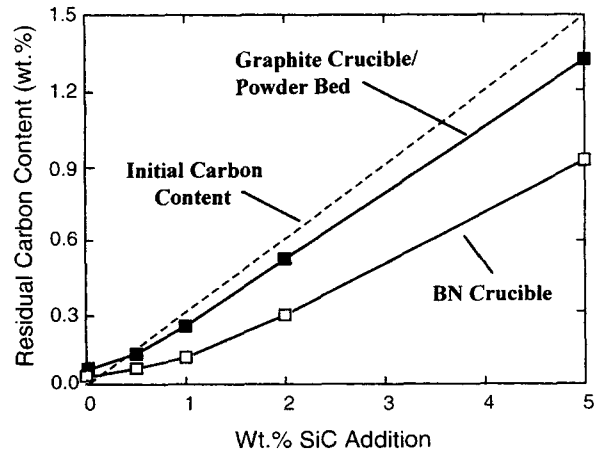

Figure 10. Amount of residual carbon in SiC/Si_3N_4 composite parts (from physically mixed powder) after pressureless sintering in different crucible environments.

(1.6 wt. % SiC), the carbon measured in the component after sintering at 1,750°C for 12 h was 0.1 wt. % and 0.40 wt. % for the BN and graphite crucible configurations, respectively. TEM analysis of these sintered materials indicates that both materials contain nanophase SiC particles in the microstructure. A TEM micrograph of the composite part that was pressureless sintered in a graphite crucible with a powder bed is shown in Figure 11. This material was found to contain both intergranular SiC (within the glassy phase) and intragranular SiC (with the β-Si_3N_4 grains). The mean equivalent circle diameters (d_{mecd}) of the intergranular and intragranular SiC were 0.22 ± 0.04 μm and 0.08 ± 0.04 μm, respectively. This size difference suggests that only the fine nanosized SiC particles are incorporated into the β-Si_3N_4 grains during the α to β transformation and growth process. As expected, TEM analysis revealed a much lower nanophase SiC content in the material sintered in the BN crucible. However, the unexpected result was that this material contained no intergranular SiC particles. The only SiC particles formed in the material were within the Si_3N_4 grains (intragranular SiC). The average size of the intragranular SiC particles was also 0.08 ± 0.04 μm. This absence of SiC particles confirms the reactivity of the SiC in the glass phase when sintering in the BN crucible environment.

In order to determine at what temperatures the SiC reacted in the BN crucible, a CO analyzer was used to analyze the N_2 atmosphere that passed through the furnace during sintering. The CO profiles for specimens made with the physical mixture of Si_3N_4 and up to 5.0 wt. % SiC are shown in Figure 12. The solid bold line is the base line CO profile for Si_3N_4 powder without any SiC addition. For this specimen, the CO content in the N_2 atmosphere was relatively low up

Figure 11. Transmission electron micrograph of a carbothermal SiC/Si_3N_4 composite part sintered in a graphite crucible/powder bed.

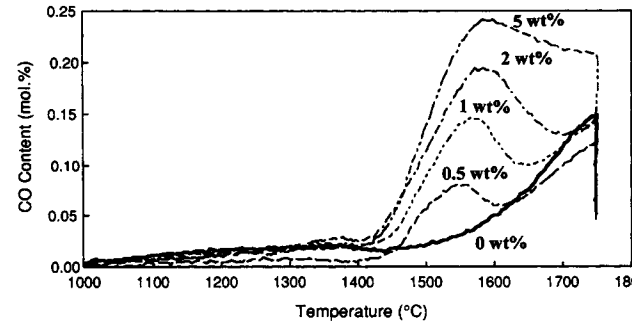

Figure 12. CO profiles as a function of temperature for SiC/Si_3N_4 physically mixed composite powders pressureless sintered in a BN crucible.

to temperatures of 1,500–1,600°C. At this point, the CO content increased reaching a maximum at 1,750°C. Once 1,750°C was reached, the CO content decreased as a function of time.

The increase in CO content at temperatures above 1,500–1,600°C is believed to be associated with the high vapor pressure of the oxide sintering additives (e.g., SiO_2). As the oxide species volatilize from the compact, they react with the graphite furnace walls to generate CO gas. For the formulations containing SiC additions, a secondary CO peak was observed during sintering. This secondary CO peak started at ~1,400–1,450°C and reached a maximum at 1,550°C–1,575°C. The amount of CO generated in this temperature range increased with proportion to the amount of SiC in the formulation.

The CO profile observed during sintering of a Y_2O_3–MgO–SiO_2–ZrO_2-based composition made with the carbothermal nanophase SiC/Si_3N_4 composite powder is shown in Figure 13. This particular lot of composite powder contained ~1.60 wt. % SiC. For comparison, the CO profiles for the components made with the physical mixture of Si_3N_4 and 0.0 and 1.0 wt. % additions of SiC are also shown. The carbothermal composite powder also exhibited a secondary CO peak. The secondary CO peak, however, was slightly

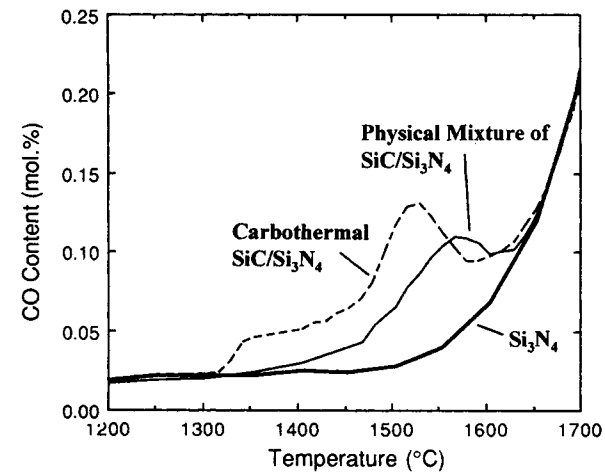

Figure 13. CO profile as a function of temperature for carbothermal and physically mixed SiC/Si_3N_4 composite powders sintered in a BN crucible.

different from that observed in the SiC/Si_3N_4 physical powder mixtures. First, the initial CO generation occurred at ~1,325°C where a small shoulder was observed on the secondary CO peak. This temperature is ~75°C lower than the initial CO generation in the Si_3N_4 powder doped with 1.0 wt. % SiC. Secondly, the secondary peak for the carbothermal composite powder reached a maximum CO output at 1,525°C. This temperature was also approximately 75–100°C lower than the maximum CO generation in the SiC/Si_3N_4 powder mixture.

The generation of CO at lower temperature for the carbothermally produced composite powder compact is most likely due to an enhanced reactivity caused by the finer SiC particle size in the carbothermal composite powder. The size of the nanophase SiC in the carbothermal powder is < 250 nm as compared to a range of 100–800 nm for the SiC in the powder mixture.

The small shoulder observed on the secondary CO peak for the carbothermal composite powder may be due to one or two sources. The first source may be a bimodal size distribution of nanophase SiC where the smallest segment of the SiC particles react first at ~1,325°C, followed by the larger nanosized particles at higher temperatures. The second possible explanation for this small shoulder is that the carbothermal powder could contain a small amount of residual carbon that was not completely removed by the postoxidation step. Even though our TEM analysis did not observe free carbon in this powder, it is possible that some residual carbon might have remained. If carbon is present, a reaction with the SiO_2 in the sintering formulation can occur at approximately 1,300°C to generate CO (Kevorkijan et al., 1992).

Thermodynamic calculations were conducted by Srinivasan (personal communication, 1993) on the Si_3N_4–Y_2O_3–MgO–SiO_2–ZrO_2 system in combination with SiC and N_2 to determine if CO evolution was possible in the observed temperature ranges. The result of this analysis indicated that a reaction between ZrO_2 and SiC is possible at temperatures of 1,450–1,500°C, yielding ZrN and CO. Even though these calculations predict the SiC to be unstable during sintering, our results show that, with the appropriate crucible environment, such as the graphite crucible/powder bed, the SiC phase can be made stable.

It is known that the local environment in a crucible filled with Si_3N_4 powder contains a high vapor pressure of SiO (Lange, 1982). When this SiO vapor comes into contact with the graphite crucible, a reaction will take place to generate CO. It is believed that a high partial pressure of CO develops inside the crucible and inhibits the reaction between the sintering additives and the nanophase SiC.

A similar thermodynamic calculation was also conducted on the Y_2O_3–Al_2O_3–SiO_2 system to determine if a SiC reaction is possible in other sintering additive systems. The thermodynamic calculations for this system predicted a reaction to generate CO at ~1,550–1,600°C. Sintering experiments using a carbothermal composite powder formulated with the Y_2O_3–Al_2O_3–SiO_2 system confirmed this result with a maximum CO peak at ~1,600°C.

The possibility of CO generation during pressureless sintering is of particular concern since it can decrease the ability to reach full density. This reduction in sintered density can occur by two possible means. First, the reaction can decrease the overall glass phase content by reducing the amount of oxygen present in the sintering formulation. A reduced amount of glass phase will slow the rate of densification. The second possibility is that the CO gas becomes trapped inside the densifying part, creating pores that cannot be eliminated during the latter stages of sintering. This phenomenon would be of particular concern for large components when densification occurred quickly and closed porosity is reached before CO generation is completed.

Carroll et al. (1994) have shown that the densification behavior of carbothermal nanophase composites under pressureless sintering conditions can be improved by the incorporation of an intermediate soak (~1,600°C) into the sintering cycle and/or through the use of low sintering temperatures. By making these modifications to the sintering cycle, it is believed that the majority of CO can be evolved when the compact still has open porosity, thus minimizing the amount of trapped CO gas.

Another easy solution to avoid the difficulties associated with CO generation is the use of a slight gas overpressure during densification. Gas pressures on the order of 0.6 MPa have successfully densified carbothermal nanophase SiC/Si_3N_4 powders for high sintering temperatures and short sintering times (Carroll et al., 1994).

Mechanical properties of nanophase SiC/Si_3N_4 composites

As an indication of the type of mechanical properties that can be obtained with carbothermal nanophase SiC/Si_3N_4 powders, the mechanical properties of composite parts densified by pressureless sintering and hot-pressing methods were evaluated. These materials were fabricated with a carbothermally produced powder containing ~1.60 wt. % SiC.

The relationship between how the average room temperature fracture strength varied with pressureless sintering conditions (i.e., temperature and time) for the Y_2O_3–Al_2O_3–SiO_2 sintering formulation is summarized in Figure 14. These

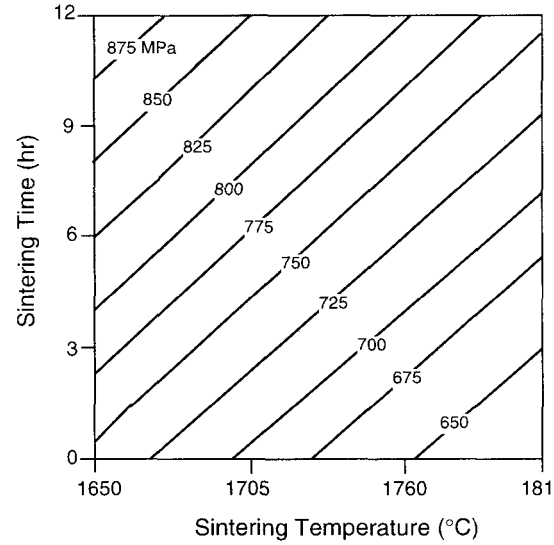

Figure 14. Contour plot of room temperature fracture strengths for pressureless sintered carbothermal SiC/Si_3N_4 composite parts as a function of sintering temperature and time in a BN crucible.

results were generated from an experimental design that investigated the optimum sintering conditions for a carbothermal composite powder (Carroll et al., 1994). The materials were sintered in a BN crucible using a two-stage sintering cycle that incorporated an intermediate hold at 1,600°C.

The results show that high-quality components could be obtained at the lower sintering temperatures and longer sintering times. For example, the average fracture strength increased from ~ 650 MPa for a sintering temperature/time of 1,815°C/3 h to ~ 875 MPa at 1,650°C/9 h. This strength trend is believed to be associated with the reaction mechanism discussed earlier. If the component is heated to high temperatures quickly so that sintering can take place in a short period of time, trapped CO gas will lower the sintered density and create defects that will reduce the strength. The material that was pressureless sintered to the highest strength of 875 MPa exhibited a sintered density of 98.5%.

The high-temperature fracture strength of a carbothermal composite (~ 1.6 wt. % SiC) made by hot pressing with 6 wt. % Y_2O_3 is summarized in Figure 15. For comparison, the high-temperature fracture strength of a Si_3N_4 material made with a high-quality commercially available di-imide powder (SNE10) is also shown. Parts fabricated from the carbothermal composite powder had significantly improved high-temperature properties over the commercially available powder. For example, at 1,250°C, the fracture strength of the parts fabricated from the carbothermal powder was 850 MPa, whereas the part fabricated from the di-imide powder exhibited a fracture strength of 650 MPa. At 1,370°C, the part composite made with the carbothermal powder was ~ 50% stronger (strength of 680 MPa) than the composite part made from the di-imide powder. It is believed that this improved high temperature fracture strength is associated with the nanophase SiC.

The effect of SiC content on the mechanical properties of carbothermal nanophase SiC/Si_3N_4 composites was investigated using hot-pressed materials containing from ~ 1.5 wt. % to 18 wt. % SiC. Hot pressing was utilized to ensure that full densification occurred, particularly for high SiC contents. The sintering formulation for this analysis was the Y_2O_3–MgO–CaO system. The effect of nanophase SiC content on the room temperature strength and fracture toughness for the carbothermal nanophase SiC/Si_3N_4 composite is shown in Figures 16 and 17, respectively. The room temperature fracture strength and toughness were found to be independent of the nanophase SiC content. The average fracture strength and toughness of this material was ~ 1,000 MPa and ~ 7.8 MPa·$m^{1/2}$, respectively.

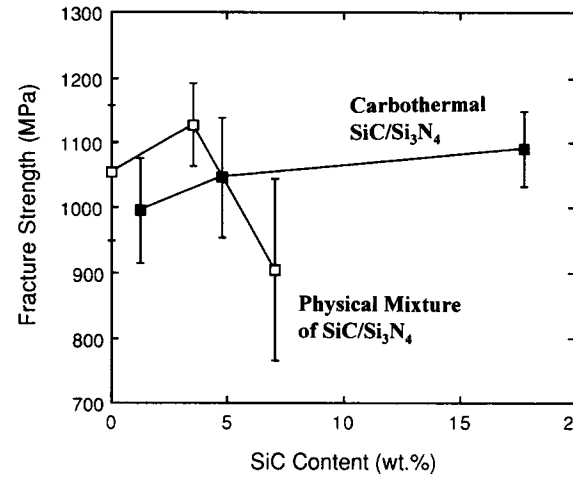

Figure 16. Room temperature fracture strength of SiC/Si_3N_4 composite parts as a function of SiC content.

These results are different from those reported by Niihara et al. (1991) and Yanai and Ishizaki (1993). Their work showed a maximum in fracture toughness and strength with SiC content. They associated this maximum in properties to fine elongated Si_3N_4 grains formed at an optimum nanophase SiC content. It is possible that this behavior was not observed in the carbothermal composites since the microstructure already contained fine, elongated Si_3N_4 grains from the Y_2O_3–MgO–CaO sintering formulation (Pyzik and Carroll, 1994).

The properties for composites made with the same formu-

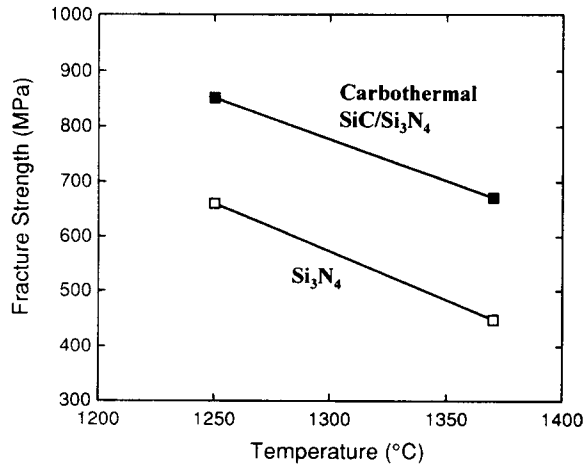

Figure 15. Fracture strength of SiC/Si_3N_4 composite and monolithic Si_3N_4 parts as a function of temperature.

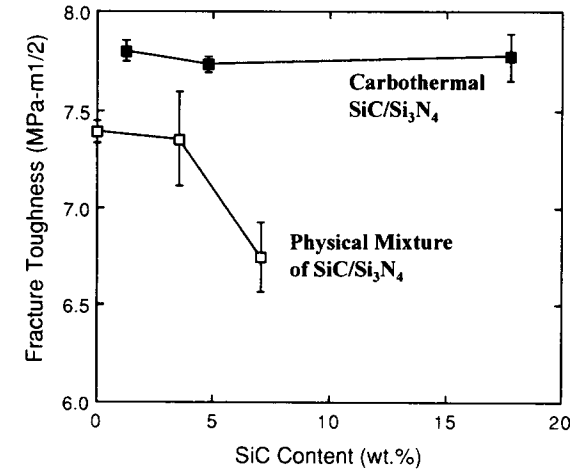

Figure 17. Room temperature fracture toughness of SiC/Si_3N_4 composite parts as a function of SiC content.

lation but with a physical mixture of SiC and Si_3N_4 are also shown in Figures 16 and 17. The average fracture strengths for these materials exhibited an apparent maximum in strength at ~3 wt. % SiC. This slight increase in strength is not believed to be a true maximum, but more likely due to strength variations caused by processing difficulties. This conclusion was made based upon the fracture toughness results that showed a linear decrease with SiC content. If a true maximum in strength occurred, a corresponding maximum in fracture toughness should have been observed (assuming constant flaw-size distribution).

The mechanical properties of the carbothermal nanophase SiC/Si_3N_4 composites made with the Y_2O_3–MgO–CaO sintering formulation were then investigated at 1,300°C. The percentage of the room temperature strength retained at 1,300°C as a function of SiC content for the carbothermal composite part is summarized in Figure 18. For comparison, the results for composite parts made from the physical mixture of SiC and Si_3N_4 are also shown. The results presented in Figure 18 indicate that the best high-temperature strength retention was obtained with the carbothermal composite part containing 3.5 wt. % SiC. At this SiC loading, the material was able to retain ~68% of its room temperature strength at 1,300°C. At higher SiC loadings, the strength retention decreased. In comparison, the high-temperature strength retention of the composite made with the physical mixture of SiC and Si_3N_4 did not change with the addition of 3.5 wt. % SiC.

The effect of nanophase SiC content on creep resistance was also evaluated by measuring the strain at failure that each material exhibited during the high-temperature strength test. A higher strain at failure corresponded to a lower creep resistance. These results are summarized in Figure 19. The carbothermal composite parts exhibited very little creep deformation at 1,300°C with a strain at failure of 0.008 for a SiC loading of 1.5 wt. % and 0.007 for a SiC loading of 18 wt. %. The composite made with the physical mixture of SiC and Si_3N_4, on the other hand, exhibited more creep deformation and had a strong dependence on SiC content.

These results indicate that the nanophase SiC can improve the high-temperature strength and creep resistance of carbothermally prepared Si_3N_4. Hirano and Niihara (1994), and Yanai et al. (1995) have suggested that improved high-temperature properties are related to the reduction in grain boundary sliding and subsequently slow crack growth, and the crystallization of the intergranular glass phase by the nanophase SiC reinforcement. The results of Ramoul-Badache and Lancin (1992) also support this conclusion. Their work has shown that the nanophase SiC enhanced devitrification of the glass phase, resulting in a densified component with a lower residual glass content. The lower amount of residual glass and the presence of nanophase SiC improved the high-temperature strength and creep resistance of their material. In our work, the fact that the carbothermal composite had significantly better creep resistance at 3.5 wt. % SiC than the composite made with the physical mixture of SiC and Si_3N_4 suggests that the glass-phase difference also contributes to the improved properties.

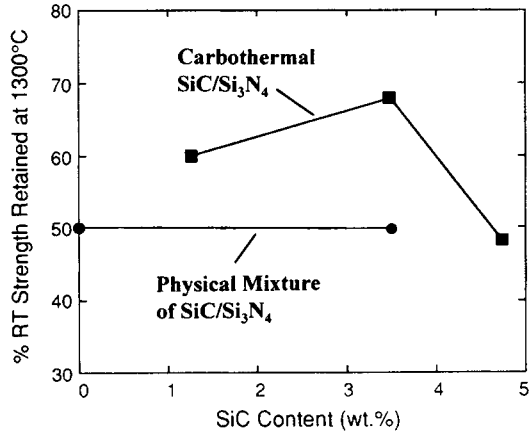

Figure 18. High temperature strength retention of SiC/Si_3N_4 composite parts at 1,300°C as a function of SiC content.

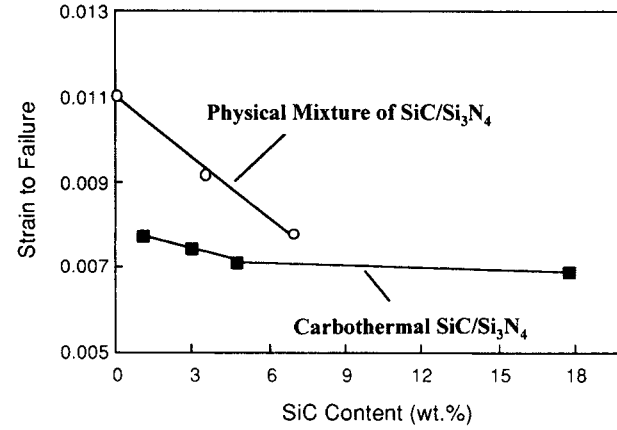

Figure 19. Relative creep resistance at 1,300°C for SiC/Si_3N_4 composite parts as a function of SiC content.

In order to investigate this issue, the glass-phase chemistry of both (carbothermally produced and physically mixed) 3.5 wt. % SiC composite parts were analyzed with X-ray diffraction, SEM, and ATEM. The X-ray diffraction results showed that each material contained β-Si_3N_4 and SiC with no evidence of glass crystallization. This result was also confirmed by ATEM analysis. SEM analysis, quantifying the amount of residual glass, showed both materials to have approximately the same glass content. The major difference between the materials was found in the EDX spectrum of the glass phase. The glass phase in the carbothermal composite was oxygen deficient with an O/Si ratio approximately 30% lower than the glass in the other material. It is suggested that the improved creep resistance of the carbothermal composite over the material made with the physical mixture of SiC and Si_3N_4 is due to this compositional difference. The lower O/Si ratio is believed to produce a glass phase that is more refractory and able to resist deformation.

Summary

Nanophase SiC/Si_3N_4 composite powders were synthesized in the presence of N_2 by the carbothermal reduction of silica in the temperature range of 1,450–1,500°C. The composite powders were characterized as high-purity, submicron Si_3N_4 powders with a homogeneous distribution of nanometer-sized particles of SiC. Reaction temperature had an effect on both the quantity and size of SiC in the nanophase

SiC/Si_3N_4 composite powder. The morphology and size of the nanophase SiC could also be controlled by the carbon source used to carbothermally reduce the silica.

The densification behavior of composite powders was examined with both pressureless and pressure-assisted densification methods. During pressureless sintering, the crucible environment was found to have a strong dependence on the stability of the SiC phase and the ability to achieve full densification in the composite powder. Under optimum pressureless sintering conditions, dense, high-strength components could be fabricated from composite powders with low SiC contents.

The effect of SiC content on the properties of SiC/Si_3N_4 composite parts was investigated at room and elevated temperatures. The results show that the fracture toughness and strength of the carbothermal composite parts at room temperature were relatively insensitive to the SiC content. The carbothermal composite parts were found to have an excellent high-temperature fracture strength and creep resistance. The optimum strength retention at 1,300°C was obtained with a composite powder having a SiC content of 3.5 wt. %. The improved creep resistance was associated with the presence of nanophase SiC particles and a glass phase with a low O/Si ratio.

Acknowledgment

This research was sponsored in part by the U.S. Department of Energy, Assistant Secretary for Energy Efficiency and Renewable Energy, Office of Transportation Technologies, as part of the Ceramic Technology Project of the Propulsion System Materials Program, under contract DE-AC05-84OR21400 with Martin Marietta Energy Systems, Inc.

Literature Cited

Akimune, Y., T. Ogasawara, and N. Hirosaki, "Influence of Starting Powder Characteristics on Mechanical Properties of SiC-Particle/Si_3N_4 Composites," *J. Ceram. Soc. Jpn.*, **100**(4), 463 (1992).

Bowen, L., R. Weston, T. Carruthers, and R. Brook, "Hot-pressing and the α-β Phase Transformation in Silicon Nitride," *J. Mater. Sci.*, **13**, 341 (1978).

Carroll, D., G. Cochran, C. Conner, D. Dunmead, G. Eisman, C. Hwang, B. Pyzik, and A. Weimer, "Development of a High Quality, Low Cost Silicon Nitride Powder," *Proc. Automotive Technol. Devel. Contractors Coordination Meeting*, Soc. of Automotive Eng., Inc., p. 405 (1995).

Carroll, D., G. Cochran, C. Conner, S. Dunmead, G. Eisman, C. Hwang, and A. Weimer, "Development of a Carbothermal Silicon Nitride Powder," Amer. Ceram. Soc. Ann. Meeting, Indianapolis, IN (1994).

Drennan, J., Q. Fan, and P. Gu, "Mechanical Property/Microstructure Relationships in a Range of Si_3N_4/SiC Composites," *Int. Symp. Ceram. Mater. Compon. Eng.*, World Scientific, Singapore, p. 298 (1995).

Hampshire, S., and K. Jack, "The Kinetics of Densification and Phase Transformation of Nitrogen Ceramics," *Proc. Br. Ceram. Soc.*, **31**, 31 (1981).

Hapke, J., and G. Ziegler, "Synthesis and Pyrolysis of Liquid Organometallic Precursors for Advanced Si-Ti-C-N Composites," *Adv. Mater.*, **7**(4), 380 (1995).

Hirano, T., and K. Niihara, "Effects of Grain Boundary Structure on Creep Behavior for Si_3N_4/SiC Composites," *Ceram. Trans.*, **44**, 211 (1994).

Hirano, T., K. Niihara, T. Ohji, and F. Wakai, "Improved Creep Resistance of Si_3N_4/SiC Nanocomposites Fabricated from Amorphous Si-C-N Powders," *J. Mater. Sci.*, **15**, 505 (1996).

Ishizaki, K., and T. Yanai, "Si_3N_4 Grain Boundary Reinforcement by SiC Nanocomposites," *Silicate Ind.*, **60**(7/8), 215 (1995).

Kennedy, P., and B. North, "The Production of Fine Silicon Carbide Powder," *Fabrication Science 3*, D. Taylor, ed., British Ceram. Soc., Shelton, UK, p. 1 (1983).

Kevorkijan, V., M. Komac, and D. Kolar, "The Influence of Preparation Conditions on the Properties of Beta SiC Powders Synthesized by Carbothermic Reduction," *Ceram. Powd. Proc. Sci. Proc. Int. Conf.*, p. 327 (1989).

Kevorkijan, V., M. Komac, and D. Kolar, "Low-Temperature Synthesis of Sinterable SiC Powders by Carbothermal Reduction of Colloidal SiO_2," *J. Mater. Sci.*, **27**(10), 2705 (1992).

Klinger, N., E. L. Strauss, and K. L. Komarek, "Reactions Between Silica and Graphite," *J. Amer. Ceram. Soc.*, **55**, 414 (1972).

Lange, F., "Volatilization Associated with the Sintering of Polyphase Si_3N_4 Materials," *J. Amer. Ceram. Soc.*, **65**, C120 (1982).

Li, H., L. Huang, and X. Fu, "The Preparation of Nanometric SiC-Si_3N_4 Composite Powders," *Proc. Int. Symp. Ceram. Compon. Eng.*, World Scientific, Singapore, p. 586 (1995).

Matsui, J., and A. Yamakawa, "Composite Silicon Nitride Sinter and Production Thereof," Eur. Patent Application #552381A1 (1992).

Newman, J., Jr., "A Review of Chevron-Notched Fracture Specimens," *Chevron Notched Specimens: Testing and Stress Analysis*, ASTM, p. 5 (1984).

Niihara, K., T. Hirano, and N. Atsushi, "Nanostructure and the Thermomechanical Properties of Silicon Nitride-Silicon Carbide Composites Fabricated From Silicon-Carbon-Nitrogen Precursors," *Funtai Funmatsu Yakin*, **36**(2), 243 (1989).

Niihara, K., K. Izaki, and A. Nakahira, "Nanocomposite Materials Based on Silicon Nitride and Silicon Carbide," *Key Eng. Mater.*, **56-57**, 319 (1991).

Niihara, K., T. Sekino, and A. Nakahira, "Ceramic Based Nanocomposites with Improved Properties and New Functions," *New Functionality Materials*, Vol. C: *Synthetic Process and Control of Functionality Materials*, Elsevier, New York, p. 751 (1993).

Pezzotti, G., and M. Sakai, "Effect of a Silicon Carbide 'Nano Dispersion' on the Mechanical Properties of Silicon Nitride," *J. Amer. Ceram. Soc.*, **77**(11), 3039 (1994).

Pyzik, A., and D. Carroll, "Technology of Self-reinforced Silicon Nitride," *Annu. Rev. Mater. Sci.*, **24**, 189 (1994).

Ramoul-Badache, K., and M. Lancin, "Si_3N_4-SiC Particulate Composites: Devitrification of the Intergranular Phase and Its Effect on Creep," *J. Eur. Ceram. Soc.*, **10**, 369 (1992).

Riedel, R., H. Kleebe, H. Schonfelder, and F. Aldinger, "A Covalent Micro/nanocomposite Resistant to High Temperature Oxidation," *Nature*, **374**, 526 (1995).

Russ, J. C., *Computer-Assisted Microscopy. The Measurement and Analysis of Images*, Plenum Press, New York, pp. 182, 192 (1990).

Sasaki, G., H. Nakase, T. Fujita, and K. Niihara, "Mechanical Properties and Microstructure of Si_3N_4 Matrix Composite with Nanometer Scale SiC Particles," *J. Ceram. Soc. Jpn.*, **100**(4), 536 (1992).

Watari, K., K. Ishizaki, and M. Kawamoto, "Behavior of Carbon in Hot Pressed Silicon Nitride Grain Boundaries and Its Influences on Mechanical Properties," *J. Ceram. Soc. Jpn.*, **96**, 127 (1988).

Wei, G. C., C. R. Kennedy, and L. A. Harris, "Synthesis of Sinterable SiC Powders by Carbothermic Reduction of Gel-derived Precursors and Pyrolysis of Polycarbosilane," *Ceram. Bull.*, **63**, 1054 (1984).

Weimer, A. W., K. J. Nilsen, G. A. Cochran, and R. P. Roach, "Kinetics of Carbothermal Reduction Synthesis of Beta Silicon Carbide," *AIChE J.*, **39**(3), 493 (1993).

Weimer, A. W., G. A. Eisman, D. W. Susnitzky, D. R. Beaman, and J. W. McCoy, "Mechanism and Kinetics of the Carbothermal Nitridation Synthesis of α-Silicon Nitride," *J. Amer. Ceram. Soc.*, in press (1997).

Yamaguchi, A., "Effects of Oxygen and Nitrogen Partial Pressures on the Stability of Metals, Carbides, Nitrides, and Oxides in Refractories which Contain Carbon," *Refractories*, **38**(4), 2 (1986).

Yanai, T., T. Hamasaki, and K. Ishizaki "High Temperature Mechanical Strength of Si_3N_4/SiC Nanocomposites Prepared From Coated Si_3N_4 Powders," *J. Ceram. Soc. Jpn.*, **103**(10), 1017 (1995).

Yanai, T., and K. Ishizaki, "Mechanical Properties of Si_3N_4 Ceramics Prepared from Carbon Coated Powders," *J. Ceram. Soc. Jpn.*, **101**(7), 764 (1993).

Zhang, S.-C., and W. R. Cannon, "Preparation of Silicon Nitride from Silica," *J. Amer. Ceram. Soc.*, **67**(10), 691 (1984).

Manuscript received Oct. 28, 1996, and revision received June 9, 1997.